Original Article

Image quality and detection efficacy of zero echo time magnetic resonance imaging on Lung-RADS 2 pulmonary ground-glass nodules in comparison to thin-slice fat-saturated T2-weighted imaging

Qiao Zou[1,2#], Qi Wan[2#], Jieqiong Liu[2#], Weiyin Vivian Liu[3], Ruolin Ding[4], Hanzhen Fang[5], Hongyan Liu[6], Xinchun Li[2], Changhong Liang[1]

[1]Department of Radiology, Guangdong Provincial People's Hospital (Guangdong Academy of Medical Sciences), Southern Medical University, Guangzhou, China; [2]Department of Radiology, The First Affiliated Hospital of Guangzhou Medical University, Guangzhou, China; [3]GE Healthcare, Beijing, China; [4]The Second Clinical Medicine School, Guangzhou Medical University, Guangzhou, China; [5]Department of Radiology, Huilai County People's Hospital, Jieyang, China; [6]The Sixth Affiliated Hospital of Guangzhou Medical University, Qingyuan People's Hospital, Qingyuan, China

Contributions: (I) Conception and design: Q Wan; (II) Administrative support: X Li, C Liang; (III) Provision of study materials or patients: Q Zou, J Liu; (IV) Collection and assembly of data: Q Zou, WV Liu; (V) Data analysis and interpretation: Q Zou, Q Wan; (VI) Manuscript writing: All authors; (VII) Final approval of manuscript: All authors.

[#]These authors contributed equally to this work.

Correspondence to: Xinchun Li, MD, PhD. Department of Radiology, The First Affiliated Hospital of Guangzhou Medical University, 151 Yanjiangxilu, Guangzhou 510120, China. Email: xinchunli@163.com; Changhong Liang, MD, PhD. Department of Radiology, Guangdong Provincial People's Hospital (Guangdong Academy of Medical Sciences), Southern Medical University, 106 Zhongshan Er Rd., Guangzhou 510080, China. Email: liangchanghong@gdph.org.cn.

Background: Widely used computed tomography (CT) screening increases the detection of pulmonary pure ground-glass nodules (pGGNs), often classified as the second category of Lung Imaging Reporting and Data System (Lung-RADS 2). Despite their low malignancy risk, these nodules pose significant challenges and necessitate accurate assessment to minimize the risk of long-term follow-ups. This study investigated the detection efficacy of zero echo time (ZTE) magnetic resonance imaging (MRI) and thin-slice fat-saturated T2-weighted imaging (T2WI-FS) on 3.0 T MRI on the predictive accuracy of invasiveness for Lung-RADS 2 pGGNs.

Methods: This prospective study enrolled 83 consecutive patients with 110 pGGNs who underwent preoperative CT and MRI scans. All CT images were assessed by artificial intelligence (AI) software and confirmed by a thoracic radiologist. Another two radiologists blind to pathology results assessed MRI for image quality (objective and subjective evaluations) and detection of pGGNs. Differences in nodule diameter, CT density and detection rate were compared within different pathological groups. The objective and subjective image quality scores were compared using the Wilcoxon signed rank test between ZTE and T2WI-FS. Interobserver agreement was calculated using the kappa coefficient. Receiver operating characteristic (ROC) curve analysis evaluated the diagnostic accuracy for distinguishing invasiveness.

Results: Among the 110 pGGNs evaluated, T2WI-FS demonstrated a higher detection rate (80.0%) compared to ZTE (51.8%). ZTE showed a superior signal-to-noise ratio (SNR) in the lung parenchyma, aorta, and peripheral lung structures, whereas T2WI-FS more effectively delineated tracheal walls and pulmonary nodules. Both observers rated ZTE higher for vascular and bronchial visibility, while T2WI-FS was better in terms of lower noise and fewer artifacts. Notably, ZTE visibility varied with pathological results, exhibiting a range from 0% in atypical adenomatous hyperplasia (AAH) to 94.1% in invasive adenocarcinoma (IAC). The key indicators for distinguishing invasive pGGNs from non-invasive ones were nodule diameter [area under the curve (AUC) =0.874], ZTE visibility (AUC =0.740), followed by CT values

(AUC =0.682) and T2WI-FS visibility (AUC =0.678).

Conclusions: MRI has the potential to detect and predict the invasiveness of pGGN. Both T2WI-FS and ZTE demonstrate reliable image quality in pulmonary imaging, each displaying strengths in visualizing pGGN. Thin-slice T2WI-FS has a superior detection rate, while ZTE better predicts histological invasiveness.

Keywords: Ground-glass nodule; zero echo time (ZTE); magnetic resonance imaging (MRI)

Submitted Mar 13, 2024. Accepted for publication Jul 05, 2024. Published online Aug 19, 2024.
doi: 10.21037/jtd-24-414
View this article at: https://dx.doi.org/10.21037/jtd-24-414

Introduction

With the prevalence of computed tomography (CT) screening, pulmonary pure ground-glass nodules (pGGNs) are increasingly being detected. The Lung Imaging Reporting and Data System (Lung-RADS) is a standardized classification system for lung cancer CT screening reports (1). pGGNs mostly belong to Lung-RADS 2 category. Despite its low malignancy risk, inaccurate classification may cause long-term follow-ups and anxiety for patients (1,2).

Local pGGNs encompass a range of benign and malignant entities, including focal inflammatory lesions (FILs), precursor glandular lesions [atypical adenomatous hyperplasia (AAH), adenocarcinoma in situ (AIS)], minimally invasive adenocarcinoma (MIA), and invasive adenocarcinoma (IAC) (3). Precursor glandular lesions are characterized by nearly 100% 5-year disease-free survival following surgery (4). However, MIA with poorly differentiated invasive patterns, such as micropapillary or solid predominant patterns, may recur or develop metachronous adenocarcinoma, requiring stricter monitoring and additional post-operation measures (5). IAC exhibits a relatively less favorable prognosis (6). Therefore, accurate prediction of pathological subtypes (e.g., invasive and non-invasive lesions) is essential for optimal patient management.

Size and CT values have been reported as predictive factors for the invasiveness of pure ground-glass opacity (pGGO), while some studies have indicated that CT density cannot effectively differentiate between invasive and preinvasive histology (7,8). Furthermore, dual-layer spectral detector CT (9) and CT-based radiomics (10,11) have been utilized to predict the invasiveness of pGGO. However, most previous studies have only included precursor lesions and invasive lesions, while FILs that are often clinically confusing have rarely been incorporated. In contrast, pulmonary magnetic resonance imaging (MRI) has emerged as a promising alternative to CT in the assessment of lung diseases, particularly for patients with lung nodules (12). Ultrashort echo time (UTE) MRI has shown promising results in lung nodule screening compared to low-dose and standard CT imaging (13,14); it has been a favorable and effective option for lung imaging, especially for those who are sensitive to radiation exposure (15). Zero echo time (ZTE) is another high-resolution pulmonary structural imaging with better image quality and shorter echo time than UTE (16). Additionally, T2-weighted imaging shows good performance on lung nodule screening (17).

To the best of our knowledge, there are few studies on the capability of ZTE for pGGN detection in comparison with thin-slice T2WI, not to mention research on the invasiveness of pGGN. Therefore, this study aimed to

Highlight box

Key findings

- The detection rate for pure ground-glass nodules (pGGNs) by thin-slice fat-saturated T2-weighted imaging (80.0%) outperformed zero echo time (ZTE) (51.8%).
- ZTE visibility was associated with pathology from 0% for atypical adenomatous hyperplasia to 94.1% for invasive adenocarcinoma.

What is known and what is new?

- Magnetic resonance imaging (MRI) is a promising tool in lung nodule screening compared to computed tomography; however, the ability of MRI to detect the invasiveness of pGGN has seldom been investigated yet.
- Our study demonstrates the potential of MRI as an additional tool in assessing pGGN with a lower false positive rate.

What is the implication, and what should change now?

- Magnetic resonance could serve as a potential alternative for examinations in eligible pGGN patients who require long-term follow-up.

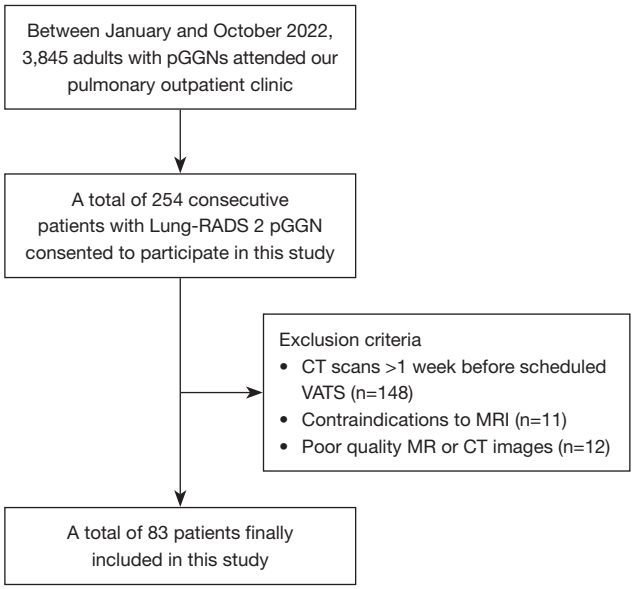

Figure 1 Flowchart of participants' enrollment. pGGNs, pulmonary pure ground-glass nodules; CT, computed tomography; VATS, video-assisted thoracoscopic surgery; MRI, magnetic resonance imaging; MR, magnetic resonance.

address this gap in knowledge of pulmonary MRI by comparing the detection rates of ZTE and thin-slice T2WI-FS for Lung-RADS 2 pGGNs and evaluating their ability to predict invasiveness on 3.0 T MRI. We present this article in accordance with the STARD reporting checklist (available at https://jtd.amegroups.com/article/view/10.21037/jtd-24-414/rc).

Methods

Patient population

This prospective study was conducted in accordance with the Declaration of Helsinki (as revised in 2013). The study was approved by the institutional review board of The First Affiliated Hospital of Guangzhou Medical University (No. 2022-63), and informed consent was taken from all the patients. The participant enrollment process is depicted in *Figure 1*. Between January and October 2022, 3,845 adult patients (aged over 18 years) visited the pulmonary outpatient clinic of The First Affiliated Hospital of Guangzhou Medical University due to the detection of pGGNs during routine health checkups. A total of 254 consecutive patients consented to participate in this study and had preoperative lung MRI after being thoroughly informed about the purpose and procedures of the study. Exclusion criteria were: (I) participants whose most recent CT scan was performed more than 1 week prior to their scheduled video-assisted thoracoscopic surgery (VATS). This ensured that the CT data were up-to-date and accurately reflected the state of the pGGNs; (II) contraindications to magnetic resonance (MR) imaging; (III) poor quality MR or CT images that hampered observation. Finally, 83 patients were included in the study, and none had participated in any previously published research.

CT examinations

Inspiratory and breath-hold CT examinations were conducted using either a 64-detector row or a 128-detector row CT scanner (Brilliance, Philips Healthcare, Amsterdam, The Netherlands; SOMATOM Definition AS, Siemens Healthcare, Erlangen, Germany) with 120 kVp and 110–270 mAs. Images were reconstructed at 1 mm thickness covering the whole lungs. These thin-slice lung images were used to identify and measure the reference nodules.

MRI examinations

MRI scans were obtained using a 3.0 T scanner (750W, GE Healthcare, Milwaukee, WI, USA). Patients were wrapped a respiratory bellows at the upper abdomen and positioned foot-first supine at the magnetic field centered along the line connecting the sternal angle and the xiphoid process. 3D respiratory-triggered ZTE was performed with a non-selective hard pulse excitation followed by 3D center-out radial sampling at a silent scanning mode, using a 32-channel body coil without contrast enhancement. we performed a shimming procedure before each sequence acquisition to ensure optimal image quality and minimize artifacts related to field inhomogeneity. Respiratory-triggering coronal and transverse T2WI-FS and transverse ZTE lung scans were carried out sequentially. Image data were prospectively collected only when the diaphragm position was within an acceptable range for about one-third of the end-expiration phase for ZTE and T2WI-FS. The parameters of ZTE and T2WI-FS are presented in *Table 1*.

Quantitative and qualitative assessment

All images were reviewed and evaluated using the Picture Archiving and Communication System (PACS, Version 5.5; Neusoft Medical, Shenyang, China) at our institution. To

Table 1 Parameters in lung MR imaging of 83 patients

Parameters	ZTE	T2WI-FS
FOV	420 mm × 420 mm	360 mm × 360 mm
Matrix	240 × 256	320 × 256
Slice thickness	1.5 mm	2.0 mm
Bandwidth	31.25 kHz	83.33 kHz
Flip angle	2°	Auto refocus
Image acquisition	Respiratory gating	Respiratory gating
TR	300–600 ms	>3,000 ms
TE	0	30–50 ms
Acquired orientation	Transverse	Transverse
Scan time, mean (range)	281 s (210–305 s)	227 s (201–246 s)

MR, magnetic resonance; ZTE, zero echo time; T2WI-FS, thin-slice fat-saturated T2-weighted imaging; FOV, field of view; TR, repetition time; TE, echo time.

objectively assess the image quality of ZTE and T2WI-FS sequences, signal intensities (SIs) of both normal structures and lung lesions were measured. Following the methodology outlined by Bae *et al.* (18), one radiologist (with 4 years of experience) placed circular regions of interest (ROIs) in specific areas including lung parenchyma, tracheal lumen and wall, aorta, subscapularis muscle, peripheral pulmonary vessel, peripheral bronchus, and lung nodules. Measurements were conducted three times for each ROI and averaged. The signal-to-noise ratios (SNRs) and contrast-to-noise ratios (CNRs) were then calculated for these structures. SNR was defined as the mean SI of the structure divided by noise, while CNR was calculated as the difference in mean SIs between the structure and lung parenchyma, divided by noise. Noise was characterized using the standard deviation (SD) of SI in the tracheal lumen.

For the qualitative assessment, separate evaluations of ZTE and T2WI-FS images were performed by two radiologists (with 10 and 8 years of experience, respectively) in a randomized order. A five-point scale was utilized to assess various parameters (18). These included visualization of pulmonary vessels and bronchi, sharpness of the diaphragmatic contour, and the presence of noise and artifacts. Overall diagnostic acceptability was also rated based on the same methodology.

Pathological analysis

The interval between pathological examination and CT/MRI scans did not exceed 1 week. Specimens were fixed in 10% neutral-buffered formalin, paraffin-embedded, and sectioned from lesion centers for hematoxylin and eosin staining. Two independent, blinded pathologists with expertise in pulmonary pathology evaluated the sections. Discrepancies were resolved through consensus to ensure accurate pathological diagnosis.

Data collection and analysis

CT images were transferred to commercial artificial intelligence (AI) software (Dr. Wise system, 1.22.07.31, Deep-wise Corporation, Hangzhou, China) for automatic detection and segmentation. The location, number, longest diameter, CT values (whole tumor measurement) and Lung-RADS scores of pGGNs were automatically generated by the AI software (19) and then assessed and confirmed on PACS with lung window settings [level, −600 Hounsfield unit (HU); width, 1,600 HU] by the fourth radiologist with 12 years of thoracic imaging experience as a reference standard for nodule detection.

The MRI images were independently reviewed on the same PACS by the same two radiologists who were blinded to the pathology results (with 10 years and 8 years of thoracic imaging experience, respectively) in a random order. Side-by-side comparison of MRI with CT scans to determine detectability of pulmonary pathologies. In cases of disagreement, a senior radiologist (with over 30 years of experience) served as an adjudicator.

Statistical analysis

The Wilcoxon signed-rank test was used to compare the differences in the SNR and CNR between ZTE and T2WI-FS for normal structures and lung nodules as well as subjective image quality scores. The weighted kappa coefficient was used to determine the inter-rater agreement for the qualitative assessment with the following established thresholds: slight (≤0.20); fair (0.21–0.40); moderate (0.41–0.60); substantial (0.61–0.80); almost perfect (0.81–1.00). The nodule diameters and CT values among different groups were compared using the Kruskal-Wallis test with a *post-hoc* test. The visibility of pGGNs among various pathological subgroups across different MRI sequences was examined for between-group differences using McNemar's test. We performed hierarchical regression analysis to evaluate the moderating effects of various imaging features on the invasiveness of pGGNs. In Model 1, we entered

Table 2 Patient and nodule characteristics

Characteristics	Values
Patient (n=83)	
Age (years)	49.8±11.8 [22–73]
Gender (female/male)	62/21
Number of nodules per patient	
1	63 (75.9)
2	14 (16.9)
3	4 (4.8)
4	2 (2.4)
Nodule (n=110)	
Diameter (mm)	9.7±4.8 [4–26]
Number of nodules per size category	
<6 mm	16 (14.6)
6–10 mm	58 (52.7)
>10 mm	36 (32.7)
Number of nodules per location	
RUL	38 (34.5)
RML	14 (12.8)
RLL	20 (18.2)
LUL	23 (20.9)
LLL	15 (13.6)
Number of nodules per surgical pathology	
FIL	10 (9.1)
AAH	4 (3.6)
AIS	19 (17.3)
MIA	60 (54.5)
IAC	17 (15.5)

Values are presented as mean ± SD [range], number, or n (%). RUL, right upper lung; RML, right middle lung; RLL, right lower lung; LUL, left upper lung; LLL, left lower lung; FIL, focal inflammatory lesion; AAH, atypical adenomatous hyperplasia; AIS, adenocarcinoma in situ; MIA, minimally invasive adenocarcinoma; IAC, invasive adenocarcinoma; SD, standard deviation.

variable CT values into the base model. In Model 2, we added diameter. In Model 3, ZTE visibility was added. A receiver operating characteristic (ROC) curve analysis and area under the curve (AUC) comparison were carried out to assess the diagnostic accuracy of pGGN. Statistical analyses were conducted using the Statistical Package for the Social Sciences (SPSS) version 25.0 (Chicago, IL, USA) and MedCalc version 18.2.1 (Ostend, Belgium). A P value less than 0.05 indicated statistical significance.

Results

Participants

A total of 83 subjects (62 women and 21 men) aged 49.8±11.8 years (range, 22–73 years) were included in this study. All pGGNs were surgically removed via thoracoscopic resection after CT and MRI scans; subsequently, they were pathologically identified and analyzed by two thoracic pathologists with results shown in *Table 2*.

Quantitative and qualitative assessment

All SNRs and CNRs are shown in *Figure 2*. SNRs of the lung parenchyma, aorta, peripheral pulmonary vessel and peripheral bronchus (P<0.001) and CNRs of the peripheral pulmonary vessel (P<0.001) were higher on ZTE than on T2WI-FS, while SNRs of the tracheal wall and lung nodule and CNRs of peripheral bronchus and lung nodule (P<0.001) were significantly higher on T2WI-FS than on ZTE. There was no inter-modality difference for SNRs of subscapularis muscle (P=0.60).

The subjective image quality of the pulmonary vessels and bronchus was considerably higher (P<0.001) on ZTE by both independent radiologists (*Figure 3*). However, the scores of noise, artifacts, and overall acceptability were higher on T2WI-FS than on ZTE (all P<0.001). There were no significantly different scores for diaphragmatic sharpness (P=0.31).

Inter-reader agreements on peripheral vessels (K=0.67 in ZTE, K=0.72 in T2WI-FS), bronchus (K=0.63 in ZTE, K=0.60 in T2WI-FS), diaphragmatic sharpness (K=0.72 in ZTE, K=0.75 in T2WI-FS), image noise (K=0.62 in ZTE, K=0.76 in T2WI-FS), artifacts (K=0.65 in ZTE.K=0.70 in T2WI-FS), and overall acceptability (K=0.62 in ZTE, K=0.64 in T2WI-FS) were substantial in both sequences.

Nodule characteristics

The characteristics of nodules in the five groups are shown in *Table 3* and *Figures 4*-7. The diameters of FIL, AAH, AIS, MIA, and IAC were 5.55±2.51, 4.50±1.08, 5.92±1.57, 8.70±2.91 and 14.82±4.53 mm, respectively. IAC showed a

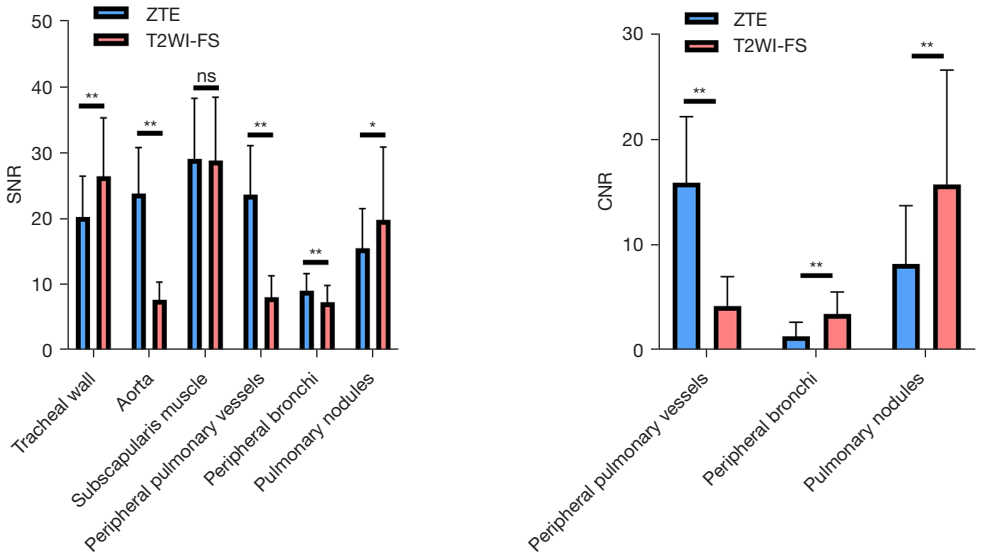

Figure 2 Comparative analysis of SNR and CNR values for different anatomical structures are shown for ZTE and T2WI-FS. Structures include lung parenchyma, tracheal wall, aorta, subscapularis muscle, peripheral vessels, peripheral bronchi, and pulmonary nodules. Statistical significance is denoted by asterisks: *, P<0.05; **, P<0.01; and 'ns' for non-significant differences. SNR, signal-to-noise ratio; CNR, contrast-to-noise ratio; ZTE, zero echo time; T2WI-FS, thin-slice fat-saturated T2-weighted imaging.

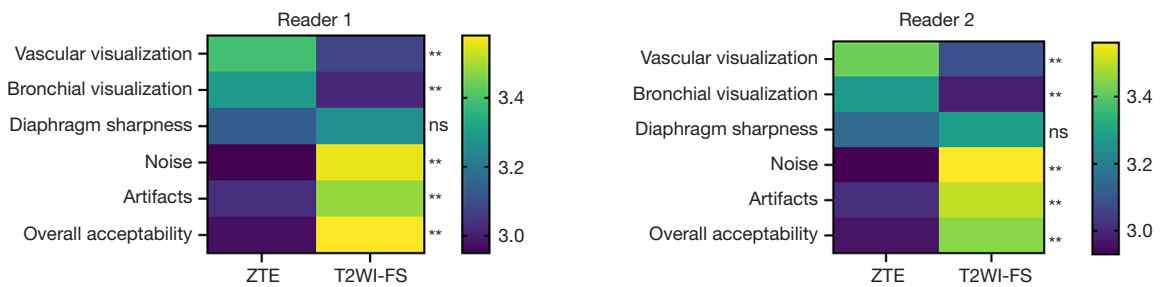

Figure 3 Reader-based qualitative assessment of ZTE and T2WI-FS image quality. The vascular visualization, bronchial visualization, diaphragm sharpness, noise, artifacts and overall acceptability were assessed. Scores range from 0 to 5, with 5 indicating the highest quality. Statistical significance is denoted by asterisks: **, P<0.01; and 'ns' for non-significant differences. ZTE, zero echo time; T2WI-FS, thin-slice fat-saturated T2-weighted imaging.

Table 3 The characteristics of nodules in different pathological entities

Variables	Pathological entities					P value
	FIL (n=10)	AAH (n=4)	AIS (n=19)	MIA (n=60)	IAC (n=17)	
CT value (HU)	−712.55±45.59	−615.60±146.77	−642.35±90.65	−615.27±82.42	−581.60±96.90	0.004
Diameter (mm)	5.55±2.51	4.50±1.08	5.92±1.57	8.70±2.91	14.82±4.53	<0.001

Data are presented as mean ± SD. FIL, focal inflammatory lesion; AAH, atypical adenomatous hyperplasia; AIS, adenocarcinoma in situ; MIA, minimally invasive adenocarcinoma; IAC, invasive adenocarcinoma; CT, computed tomography; HU, Hounsfield unit; SD, standard deviation.

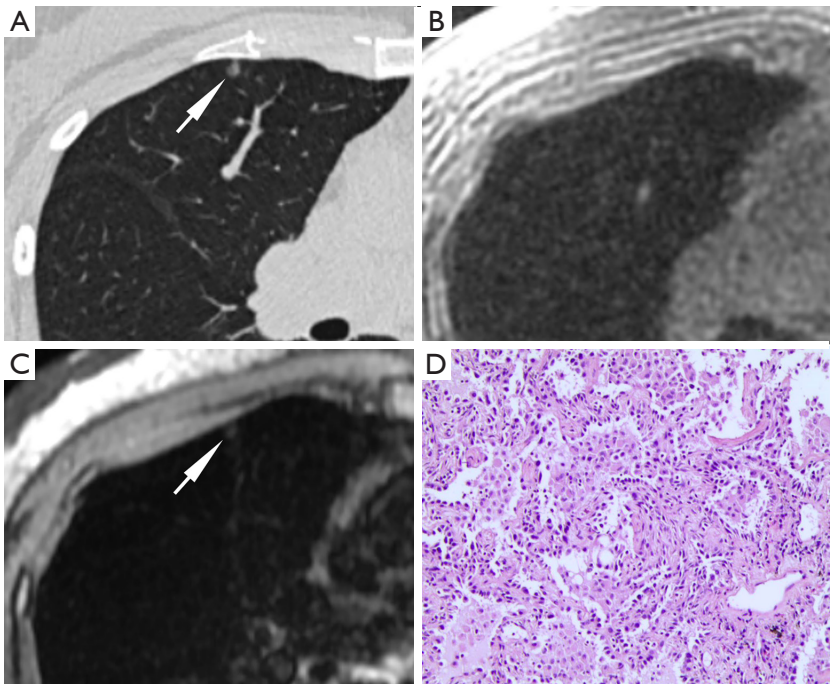

Figure 4 A 40-year-old female patient. CT scan shows a 4 mm × 3 mm pure ground-glass nodule (A) in the upper right lung. It is not visible on ZTE (B) but can be seen on T2WI-FS (C). Histopathological confirmation reveals AAH (HE ×200, D). Arrows indicate the pure ground-glass nodule. CT, computed tomography; ZTE, zero echo time; T2WI-FS, thin-slice fat-saturated T2-weighted imaging; AAH, atypical adenomatous hyperplasia; HE, hematoxylin and eosin.

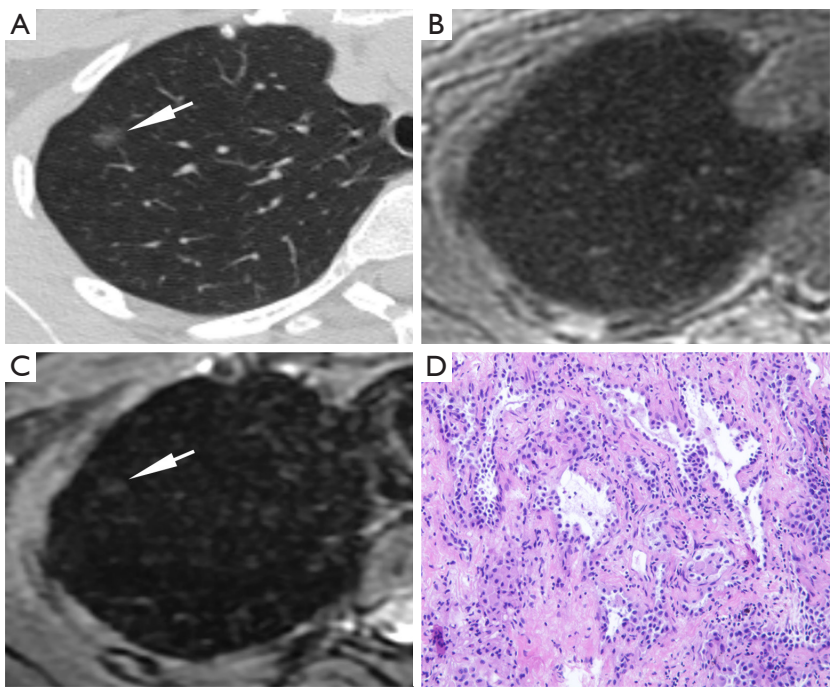

Figure 5 A 45-year-old female patient. CT scan shows an 8 mm × 6 mm pure ground-glass nodule (A) in the upper right lung. It is visible on T2WI-FS (C) but not on ZTE (B). Histopathological confirmation reveals AIS (HE ×200, D). Arrows indicate the pure ground-glass nodule. CT, computed tomography; T2WI-FS, thin-slice fat-saturated T2-weighted imaging; ZTE, zero echo time; AIS, adenocarcinoma in situ; HE, hematoxylin and eosin.

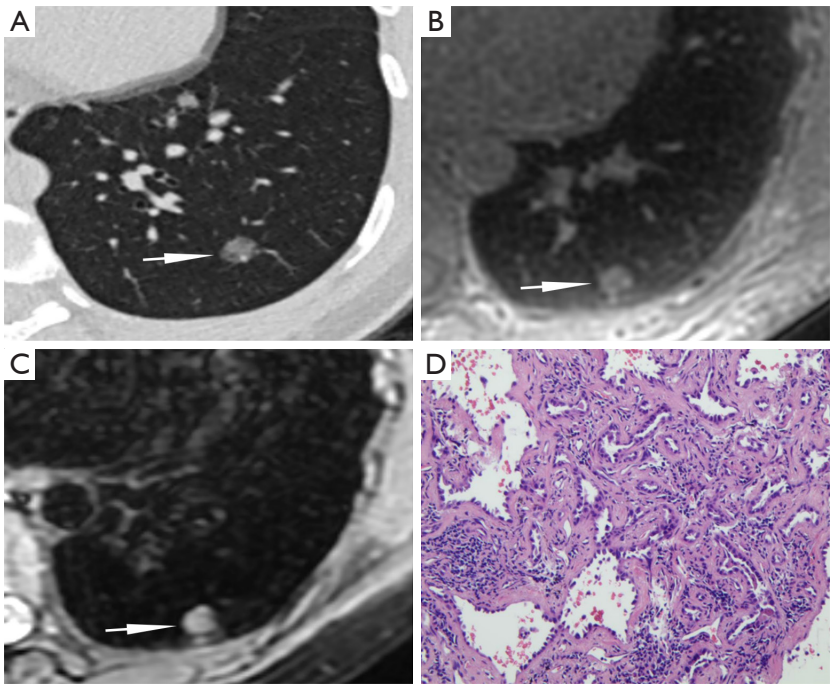

Figure 6 A 30-year-old female patient. CT scan shows a 10 mm × 9 mm pure ground-glass nodule (A) in the lower left lung. It is visible on both ZTE (B) and T2WI-FS (C). Histopathological confirmation reveals MIA (HE ×200, D). Arrows indicate the pure ground-glass nodule. CT, computed tomography; ZTE, zero echo time; T2WI-FS, thin-slice fat-saturated T2-weighted imaging; MIA, minimally invasive adenocarcinoma; HE, hematoxylin and eosin.

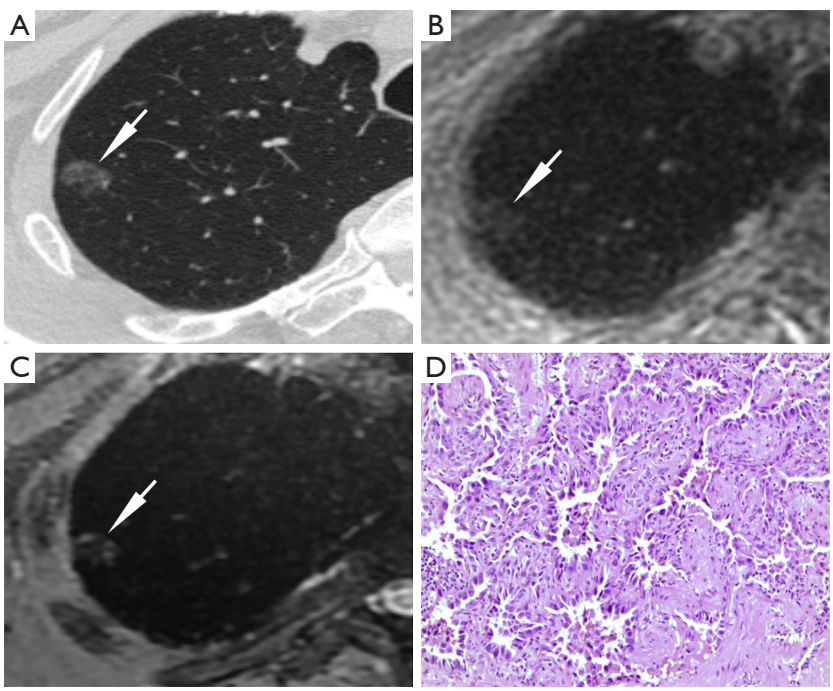

Figure 7 A 65-year-old male patient. CT scan shows a 14 mm × 12 mm pure ground-glass nodule (A) in the upper right lung. It is visible on both ZTE (B) and T2WI-FS (C). Histopathological confirmation reveals IAC (grade 2) (HE ×200, D). Arrows indicate the pure ground-glass nodule. CT, computed tomography; ZTE, zero echo time; T2WI-FS, thin-slice fat-saturated T2-weighted imaging; IAC, invasive adenocarcinoma; HE, hematoxylin and eosin.

Table 4 Association between pathological entities and visibility on MRI

Variables	ZTE, n (%)				T2WI-FS, n (%)			
	Invisible	Visible	Total	P value	Invisible	Visible	Total	P value
FIL	8 (80.0)	2 (20.0)	10	<0.001	5 (50.0)	5 (50.0)	10	0.001
AAH	4 (100.0)	0 (0.0)	4		2 (50.0)	2 (50.0)	4	
AIS	15 (78.9)	4 (21.1)	19		8 (42.1)	11 (57.9)	19	
MIA	25 (41.7)	35 (58.3)	60		6 (10.0)	54 (90.0)	60	
IAC	1 (5.9)	16 (94.1)	17		1 (5.9)	16 (94.1)	17	
Total	53 (48.2)	57 (51.8)	110		22 (20.0)	88 (80.0)	110	

MRI, magnetic resonance imaging; ZTE, zero echo time; T2WI-FS, thin-slice fat-saturated T2-weighted imaging; FIL, focal inflammatory lesion; AAH, atypical adenomatous hyperplasia; AIS, adenocarcinoma in situ; MIA, minimally invasive adenocarcinoma; IAC, invasive adenocarcinoma.

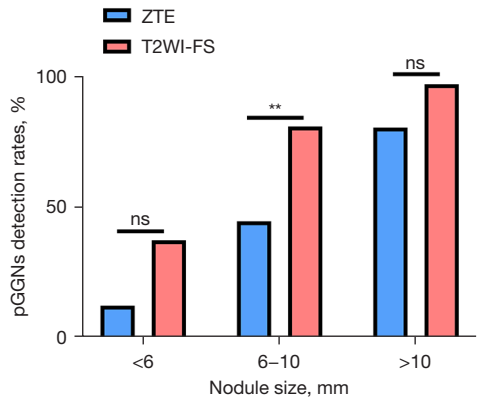

Figure 8 Detection rates of pGGNs by nodule size. The detection rates for ZTE and T2WI-FS are compared across three nodule size categories: less than 6 mm, 6 to 10 mm, and greater than 10 mm. Statistical significance is denoted by asterisks: **, P<0.01, and 'ns' for non-significant differences. ZTE, zero echo time; T2WI-FS, thin-slice fat-saturated T2-weighted imaging; pGGNs, pulmonary pure ground-glass nodules.

significantly larger diameter than MIA, AIS, AAH, and FIL (all P<0.001), and MIA had a significantly larger diameter than AIS, AAH, and FIL (P=0.001, 0.007, 0.003). No statistical differences were observed in comparisons between the other groups.

The CT values of FIL, AAH, AIS, MIA, and IAC were respectively −712.55±45.59, −615.60±146.77, −642.35±90.65, −615.27±82.42 and −581.60±96.90 in the unit of HU. AAH, MIA, and IAC showed significantly higher CT values than FIL (P=0.04, P=0.001, P<0.001, respectively), and IAC had significantly higher CT values than AIS (P=0.03). No statistical differences were observed in comparisons between the other groups.

MRI detection rate for pGGN

Among 110 pGGNs, the detection rates of ZTE and thin-sliced T2WI-FS were respectively 51.8% (57/110) and 80.0% (88/110). A significant difference in visibility was observed across the pathological entities on both ZTE MRI (P<0.001 for the overall comparison) and T2WI-FS (P=0.001 for the overall comparison). The visibility for AAH, AIS, MIA and IAC showed an increasing detectability ranging from low to high in alignment with the invasiveness. T2WI-FS demonstrated a universally higher detection rate across all pathologies compared to ZTE, with notable effectiveness in identifying MIA (90.0%) and IAC (94.1%). Even in cases of AAH, where ZTE showed no visibility, T2WI-FS was able to detect 50.0% of these nodules (*Table 4*).

According to nodule size, the detection rates of ZTE and thin-sliced T2WI-FS were respectively 12.5% and 37.5% for pGGNs <6 mm, 44.8% and 81.0% for 6–10 mm, and 80.6% and 97.2% for >10 mm (*Figure 8*). Inter-reader agreement on the detection rate for pGGNs was substantial for both ZTE (K=0.71, P<0.001) and T2WI-FS (K=0.69, P<0.001).

Hierarchical regression analysis

The result of the hierarchical regression analysis of the imaging features predicting invasiveness of pGGNs is shown in *Table 5*. In the first model, the CT value significantly

Table 5 Hierarchical regression analysis of imaging features predicting invasiveness of pGGNs

Variables	Model 1			Model 2			Model 3		
	B	P	β	B	P	β	B	P	β
Constant	1.539	<0.001**	–	0.881	0.003**	–	0.682	0.02*	–
CT value	0.001	0.005**	0.266	0.001	0.02*	0.19	0.001	0.13	0.131
Diameter				0.043	<0.001**	0.447	0.034	<0.001**	0.354
ZTE visibility							0.197	0.02*	0.215
R^2	0.071			0.264			0.297		
F value	8.212, P=0.005			19.221, P<0.001			14.925, P<0.001		
ΔR^2	0.071			0.194			0.033		
ΔF value	8.212, P=0.005			28.164, P<0.001			4.924, P=0.02		

*, P<0.05; **, P<0.01. pGGNs, pulmonary pure ground-glass nodules; B, unstandardized coefficients; β, standardized coefficients; CT, computed tomography; ZTE, zero echo time.

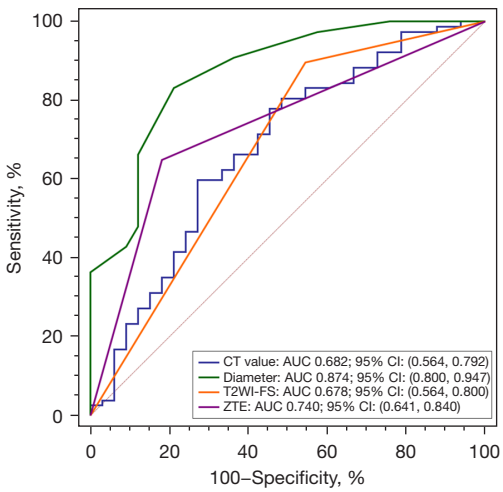

Figure 9 AUC comparison of diameter, CT value, ZTE visibility and T2WI-FS visibility in distinguishing invasiveness of pGGNs. CT, computed tomography; AUC, area under the curve; CI, confidence interval; T2WI-FS, thin-slice fat-saturated T2-weighted imaging; ZTE, zero echo time; pGGNs, pulmonary pure ground-glass nodules.

explained 7.1% of the variance in ICA + MIA pathology (R^2=0.071, F=8.212, P=0.005). In the second model, the inclusion of nodule diameter significantly increased the explanatory power to 26.4% (R^2=0.264, F=19.221, P<0.001). In the third model, the addition of ZTE visibility further improved the model, explaining 29.7% of the variance with significant changes in R^2 of 3.3% (F=14.925, P=0.02).

Diagnostic performance of image parameters

The diameter had the highest diagnostic performance on differentiating invasive pGGNs from non-invasive ones [AUC =0.874, 95% confidence interval (CI): 0.800–0.947], followed by ZTE-MRI (AUC =0.740, 95% CI: 0.641–0.840), while the CT values (AUC =0.682, 95% CI: 0.564–0.792) and T2WI-FS (AUC =0.678, 95% CI: 0.564–0.800) exhibited relatively lower AUCs. The diagnostic performance of diameter was significantly better than the other three indicators (P=0.005, 0.006, <0.001), while the differences among the other indicators were not statistically significant (*Figure 9*).

Discussion

The inherent properties of lung tissue, such as low proton density and short T2 relaxation time, have posed significant challenges for effective MR imaging. Advancements in MRI technology have led to the development of short T2-sensitive techniques like ZTE, which captures signals from rapidly decaying tissues by employing extremely short echo times, minimizing signal loss and providing greater detail and contrast in lung tissue imaging. While ZTE and traditional T2WI have shown promise in lung nodule detection (13,14,17), comparative analyses of these sequences and their efficacy in assessing the invasiveness of pGGNs remain underexplored. The present study first compared the values of ZTE and thin-slice T2WI-FS in detecting and predicting the invasiveness of Lung-RADS

2 pGGNs on 3.0 T MRI. Our findings revealed that ZTE exhibited a greater potential in predicting the histological invasiveness of pGGNs, while T2WI-FS demonstrated a higher detection rate for pGGNs.

Our analysis encompassed both subjective and objective assessments of image quality across the two sequences. The study demonstrated substantial inter-rater agreement in the subjective evaluation of pulmonary tissues using either ZTE-MRI or T2WI-FS, indicating both sequences exhibit good reproducibility and reliability for lung MR imaging. Objectively, ZTE displayed significantly higher SNR and CNR in lung parenchyma and pulmonary vessels, underscoring its enhanced capability in delineating these structures. Conversely, T2WI-FS revealed superior SNR and CNR for lung nodules, highlighting its effectiveness in nodule characterization. This indicates that different sequences possess unique advantages, necessitating their integrated use in imaging protocols. Although UTE is recommended for lung MRI applications due to its excellent assessment of lung parenchyma (12,20), T2WI-FS is indispensable for detecting and monitoring lung nodules in clinical practice.

The current study delineated invasive from preinvasive pGGNs using nodule size and CT density, achieving AUC of 0.874 and 0.682, respectively, underscoring the diagnostic utility of these parameters. An increase in the size of pGGNs correlates with a heightened risk of malignancy, a finding consistent with prior studies (21,22). While our results regarding CT values in differentiating pGGNs' pathological entities resonate with several studies (21,23), they diverge from others (8), suggesting a complex landscape of diagnostic markers. Of note, most prior CT studies relied on manual measurements, whereas automatic measure was carried out in our study. This methodological refinement aimed to minimize subjective variability, enhancing the objectivity and accuracy of our results.

A novel aspect of our study was the notable association of ZTE visibility with the histological invasiveness of pGGNs. ZTE visibility offered slightly better diagnostic performance in distinguishing between non-invasive and invasive pGGNs (AUC =0.740) compared to CT density (AUC =0.682) and T2WI-FS (AUC =0.678). However, its diagnostic performance did not exceed the predictive power of nodule diameter, which achieved the highest AUC value of 0.874. This reaffirms the diameter of pGGNs as a critical determinant in evaluating their potential invasiveness. The association of ZTE visibility with histological invasiveness highlights its potential utility as a complementary imaging technique. Larger and denser nodules are more likely to be detected on ZTE, which suggests a higher probability of malignancy. Nevertheless, the absence of a lesion on ZTE might not completely exclude the possibility of malignancy, as smaller or less dense nodules may not be visible despite their invasive nature.

We conducted a hierarchical regression analysis to further clarify the relationship between nodule size, density, and ZTE visibility. Our findings suggest that ZTE-MRI provides additional insights into nodule invasiveness, even when nodule diameter and CT values are considered. This layered approach to regression analysis reinforces the complementary strengths of CT and MRI in the comprehensive evaluation of pGGNs.

Several limitations of our study still need to be considered. Firstly, a relatively small sample size at a single hospital may limit the generalization of our findings. Secondly, we did not compare with conventional T1-weighted images (T1WI), for UTE with superior performance on lung imaging to standard post-contrast T1WI (15). Thirdly, an inherent and unavoidable limitation presented in our study population was exclusively including patients undergoing surgery to have histological results as reference. This selection criterion may introduce bias and cannot represent the broader spectrum of patients with pGGNs, potentially affecting the applicability of our results to non-surgical cases. Last but not least, although radiologists were blinded to pathology results, MR images were directly compared with CT images, which was necessary as noise on ZTE could sometimes be confused with ground-glass opacities. Future research should focus on improving the SNR of ZTE to reduce such confusion and evaluate MRI's ability to detect and assess pGGN when radiologists are blinded to CT images. However, this study is significant in demonstrating that MRI can serve as a viable follow-up tool for pGGN confirmed by CT, providing a non-ionizing alternative for long-term monitoring and potentially reducing radiation exposure from repeated CT scans.

Conclusions

Our study highlights the complementary strengths of thin-slice T2WI-FS and ZTE sequences in the imaging of pulmonary ground glass nodules. T2WI-FS excels in detection rate, making it a valuable tool for identifying pGGNs, while ZTE provides superior insight into the histological invasiveness of these nodules. In clinical practice, the combined use of T2WI and ZTE is recommended to

leverage their respective advantages, offering a comprehensive, non-radiative approach for evaluating pGGNs.

Acknowledgments

Funding: This work was supported by the Foundation of Guangzhou Municipal Science and Technology Bureau (Nos. 2024A03J1229, 202201020456), the State Key Laboratory of Respiratory Diseases (No. SKLRD-OP-202311), and the Student Innovation Capability Enhancement Program of the Second Clinical College of Guangzhou Medical University (No. 02-408-2304-02077XM).

Footnote

Reporting Checklist: The authors have completed the STARD reporting checklist. Available at https://jtd.amegroups.com/article/view/10.21037/jtd-24-414/rc

Data Sharing Statement: Available at https://jtd.amegroups.com/article/view/10.21037/jtd-24-414/dss

Peer Review File: Available at https://jtd.amegroups.com/article/view/10.21037/jtd-24-414/prf

Conflicts of Interest: All authors have completed the ICMJE uniform disclosure form (available at https://jtd.amegroups.com/article/view/10.21037/jtd-24-414/coif). W.V.L. is an employee of GE Healthcare, Beijing, China. The other authors have no conflicts of interest to declare.

Ethical Statement: The authors are accountable for all aspects of the work in ensuring that questions related to the accuracy or integrity of any part of the work are appropriately investigated and resolved. This study was conducted in accordance with the Declaration of Helsinki (as revised in 2013). The study was approved by the institutional ethics board of The First Affiliated Hospital of Guangzhou Medical University (No. 2022-63), and informed consent was taken from all the patients.

References

1. Chelala L, Hossain R, Kazerooni EA, et al. Lung-RADS Version 1.1: Challenges and a Look Ahead, From the AJR Special Series on Radiology Reporting and Data Systems. AJR Am J Roentgenol 2021;216:1411-22.
2. ACoR. Lung-Screening Reporting and Data System (LungRADS) Version 1.1. 2019. Available online: https://www.acr.org/-/media/ACR/Files/RADS/Lung-RADS/LungRADSAssessmentCategoriesv1-1.pdf?la=en
3. Chang YC, Chen PT, Hsieh MS, et al. Discrimination of invasive lung adenocarcinoma from Lung-RADS category 2 nonsolid nodules through visual assessment: a retrospective study. Eur Radiol 2024;34:3453-61.
4. Yotsukura M, Asamura H, Motoi N, et al. Long-Term Prognosis of Patients With Resected Adenocarcinoma In Situ and Minimally Invasive Adenocarcinoma of the Lung. J Thorac Oncol 2021;16:1312-20.
5. Jia M, Yu S, Cao L, et al. Clinicopathologic Features and Genetic Alterations in Adenocarcinoma In Situ and Minimally Invasive Adenocarcinoma of the Lung: Long-Term Follow-Up Study of 121 Asian Patients. Ann Surg Oncol 2020;27:3052-63.
6. Van Schil PE, Asamura H, Rusch VW, et al. Surgical implications of the new IASLC/ATS/ERS adenocarcinoma classification. Eur Respir J 2012;39:478-86.
7. Lee HY, Choi YL, Lee KS, et al. Pure ground-glass opacity neoplastic lung nodules: histopathology, imaging, and management. AJR Am J Roentgenol 2014;202:W224-33.
8. Fu F, Zhang Y, Wang S, et al. Computed tomography density is not associated with pathological tumor invasion for pure ground-glass nodules. J Thorac Cardiovasc Surg 2021;162:451-459.e3.
9. Yu Y, Fu Y, Chen X, et al. Dual-layer spectral detector CT: predicting the invasiveness of pure ground-glass adenocarcinoma. Clin Radiol 2022;77:e458-65.
10. Zhu YQ, Liu C, Mo Y, et al. Radiomics for differentiating minimally invasive adenocarcinoma from precursor lesions in pure ground-glass opacities on chest computed tomography. Br J Radiol 2022;95:20210768.
11. Zhu M, Yang Z, Wang M, et al. A computerized tomography-based radiomic model for assessing the invasiveness of lung adenocarcinoma manifesting as

ground-glass opacity nodules. Respir Res 2022;23:96.
12. Hatabu H, Ohno Y, Gefter WB, et al. Expanding Applications of Pulmonary MRI in the Clinical Evaluation of Lung Disorders: Fleischner Society Position Paper. Radiology 2020;297:286-301.
13. Ohno Y, Takenaka D, Yoshikawa T, et al. Efficacy of Ultrashort Echo Time Pulmonary MRI for Lung Nodule Detection and Lung-RADS Classification. Radiology 2022;302:697-706.
14. Ohno Y, Koyama H, Yoshikawa T, et al. Standard-, Reduced-, and No-Dose Thin-Section Radiologic Examinations: Comparison of Capability for Nodule Detection and Nodule Type Assessment in Patients Suspected of Having Pulmonary Nodules. Radiology 2017;284:562-73.
15. Renz DM, Herrmann KH, Kraemer M, et al. Ultrashort echo time MRI of the lung in children and adolescents: comparison with non-enhanced computed tomography and standard post-contrast T1w MRI sequences. Eur Radiol 2022;32:1833-42.
16. Bae K, Jeon KN, Hwang MJ, et al. Comparison of lung imaging using three-dimensional ultrashort echo time and zero echo time sequences: preliminary study. Eur Radiol 2019;29:2253-62.
17. Meier-Schroers M, Homsi R, Gieseke J, et al. Lung cancer screening with MRI: Evaluation of MRI for lung cancer screening by comparison of LDCT- and MRI-derived Lung-RADS categories in the first two screening rounds. Eur Radiol 2019;29:898-905.
18. Bae K, Jeon KN, Hwang MJ, et al. Respiratory motion-resolved four-dimensional zero echo time (4D ZTE) lung MRI using retrospective soft gating: feasibility and image quality compared with 3D ZTE. Eur Radiol 2020;30:5130-8.
19. Qi LL, Wu BT, Tang W, et al. Long-term follow-up of persistent pulmonary pure ground-glass nodules with deep learning-assisted nodule segmentation. Eur Radiol 2020;30:744-55.
20. Ohno Y, Koyama H, Yoshikawa T, et al. Pulmonary high-resolution ultrashort TE MR imaging: Comparison with thin-section standard- and low-dose computed tomography for the assessment of pulmonary parenchyma diseases. J Magn Reson Imaging 2016;43:512-32.
21. Chu ZG, Li WJ, Fu BJ, et al. CT Characteristics for Predicting Invasiveness in Pulmonary Pure Ground-Glass Nodules. AJR Am J Roentgenol 2020;215:351-8.
22. Hsu WC, Huang PC, Pan KT, et al. Predictors of Invasive Adenocarcinomas among Pure Ground-Glass Nodules Less Than 2 cm in Diameter. Cancers (Basel) 2021;13:3945.
23. Qi L, Xue K, Li C, et al. Analysis of CT morphologic features and attenuation for differentiating among transient lesions, atypical adenomatous hyperplasia, adenocarcinoma in situ, minimally invasive and invasive adenocarcinoma presenting as pure ground-glass nodules. Sci Rep 2019;9:14586.

Cite this article as: Zou Q, Wan Q, Liu J, Liu WV, Ding R, Fang H, Liu H, Li X, Liang C. Image quality and detection efficacy of zero echo time magnetic resonance imaging on Lung-RADS 2 pulmonary ground-glass nodules in comparison to thin-slice fat-saturated T2-weighted imaging. J Thorac Dis 2024;16(8):5167-5179. doi: 10.21037/jtd-24-414